Supporting Information

Tuning Macrocyclic Thermoelectrics via Thiophene Regioisomerism

Mona Alshammari,[ab†] Asma Alajmi,[ca†] Bashayr Alanazi,[da] Alotaibi Hanadi,[ae] Adel Alrehaili [af], Alaa Al-Jobory,[a] Colin Lambert,[a*] and Ali Ismael[ag*]

[a.] Physics Department, Lancaster University, Lancaster, LA1 4YB, UK.
[b.] Department of Physics, College of Science, University of Hafr Al Batin, Al Jamiah District, Hafar Al Batin 39524, Eastern Province, Saudi Arabia.
[c.] Department of Physics, College of Science and Humanities in Al-Kharj, Prince Sattam Bin Abdulaziz University, Al-Kharj 11942, Saudi Arabia
[d.] Northren border University
[e.] Department of Physics, College of Science and Humanities, Shaqra University, Al-Dawadimi Road, Riyadh Province 11961, Saudi Arabia.
[f.] Physics Department, Faculty of Science, Islamic University of Madinah, Madinah, 42351, Saudi Arabia.
[g.] Department of Physics, College of Education for Pure Science, Tikrit University, Tikrit, Iraq.

† These authors contributed equally to this work

* c.lambert@lancaster.ac.uk , and Ali Ismael: k.ismael@lancaster.ac.uk

Contents

1. DFT and transport calculations

1.1 Introduction

This study focuses on four π – conjugated macrocyclic molecules *BMC1*, *BMC2*, *TMC3*, and *TMC4* designed to explore quantum interference effects in molecular junctions. As illustrated in **Figure S 1**, these molecules differ in their structural symmetry, anchoring positions, and central aromatic units. *BMC1* and *BMC2* are benzene-based systems with *meta*- and hybrid *para/meta*-connectivity, respectively. In contrast, *TMC3* and *TMC4* incorporate a thiophene core, with differences in anchoring symmetry and path length. These structural variations enable a systematic analysis of how molecular architecture influences quantum transport behaviour. Table S1 summarises the IUPAC names and brief descriptions of these simulated molecules.

To systematically investigate how molecular architecture influences QI and charge transport, our study is divided into two parts. Part 1 focuses on conventional DFT analysis of the original molecular structures and compares the calculated transmission and Seebeck coefficients with experimental data. Part 2 explores the impact of modifying the sulfur position within the thiophene, aiming to understand how such changes influence interference patterns and transport properties.

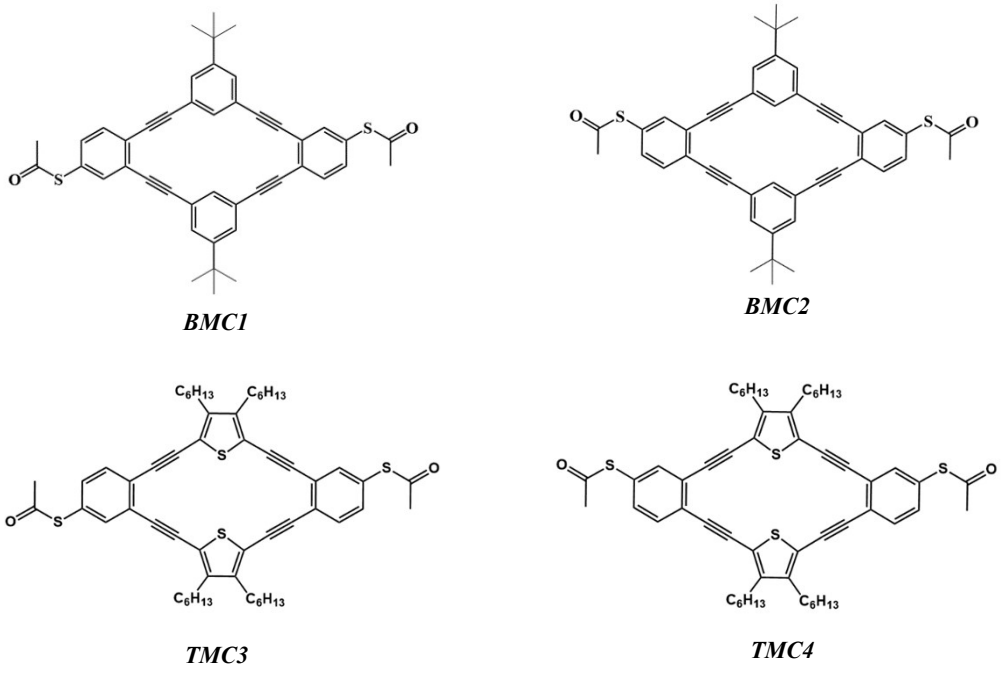

Figure S 1: Chemical structures of macrocycles . Macrocycles and exhibit symmetric conjugated backbones, while and show asymmetric designs due to substitution and path differences.

Table S 1: IUPAC names and descriptions of the four simulated macrocyclic molecules (*BMC1–TMC4*).

Molecule	IUPAC name	Description
BMC1	4,4′-[(1,3-phenylene)bis(ethyne-2,1-diyl)]bis(benzenethiol)	*Meta*-connected oligo(phenylene ethynylene) with terminal thiol groups.
BMC2	4-[[(4-mercaptophenyl)ethynyl]phenyl]ethynyl]benzenethiol	Hybrid *para/meta* connectivity structure in the OPE3 framework.
TMC3	2,5-Bis([4-[(4-mercaptophenyl)ethynyl]phenyl]ethynyl)thiophene	Thiophene-based conjugated system for comparison with benzene analogs.
TMC4	2,5-Bis([4-[(4-mercaptophenyl)ethynyl]phenyl]ethynyl)thiophene	Similar to *TMC3* but differs in anchoring configuration and interference patterns.

1.2 Optimised DFT structures of isolated molecules

Density functional theory (DFT) [1–3] calculations were performed using the SIESTA code to obtain the optimised geometries of all isolated macrocyclic molecules presented in this study. The geometries were relaxed until the atomic forces were reduced below $0.01\ eV/A^o$. A double-zeta plus polarization basis set (DZP) with a 250 Rydberg energy cut-off was employed, and the generalized gradient approximation (GGA) was used as the exchange-correlation functional. These optimised structures serve as the basis for further electronic and transport property calculations. The DFT-optimised geometries of the macrocycles are presented in **Figure S 2**, which were analysed to identify specific connectivity configurations associated with high electrical conductance (constructive quantum interference, CQI) and low conductance (destructive quantum interference, DQI).

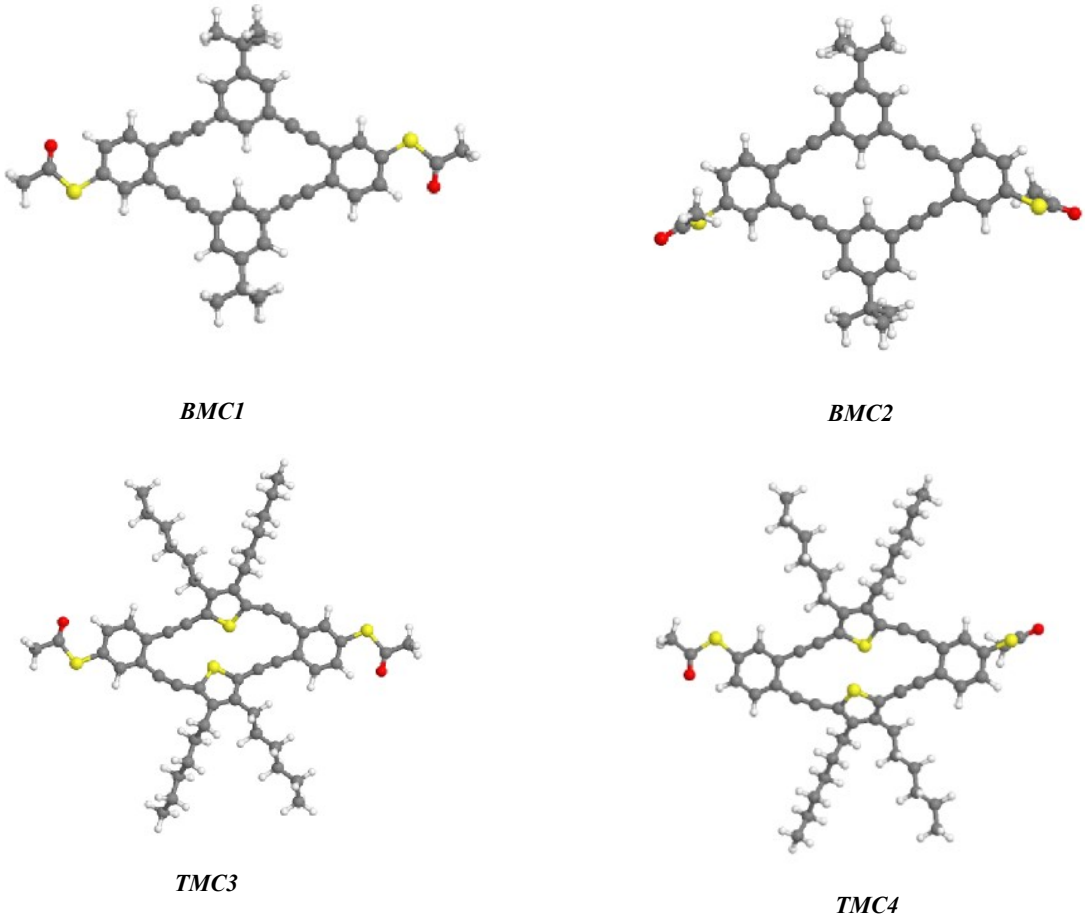

Figure S 2: Fully relaxed isolated molecules of the same macrocycles obtained from DFT optimisation, revealing their conformational flexibility and overall topology before transport calculations.

1.3 Frontier molecular orbitals

To explore the electronic properties of the molecules under study, we analysed their frontier molecular orbitals (FMOs), including the highest occupied molecular orbital (HOMO), the lowest unoccupied molecular orbital (LUMO), and the neighbouring orbitals (HOMO–1, HOMO–2, LUMO+1, LUMO+2). These orbitals provide insight into the phase and amplitude distributions that influence charge transport behaviour. The blue and red regions in the wavefunction plots represent negative and positive amplitudes, respectively. The wave functions of *BMC1*, *BMC2*, *TMC3*, and *TMC4* are illustrated in **Figure S 3** to **Figure S 6**.

BMC1

$E_F = -4.01\ eV$

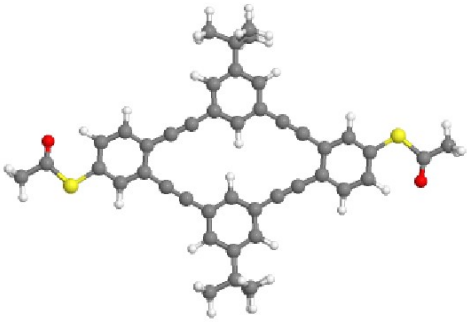

$HOMO = -4.62\ eV$

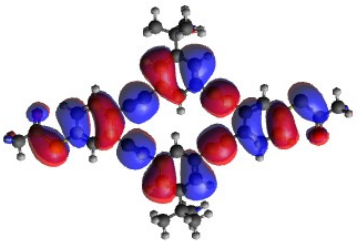

$LUMO = -2.36\ eV$

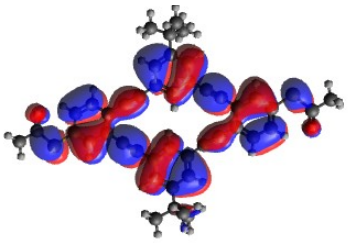

$HOMO - 1 = -4.81\ eV$

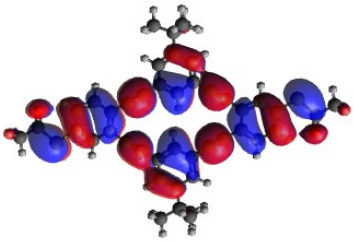

$LUMO + 1 = -2.13\ eV$

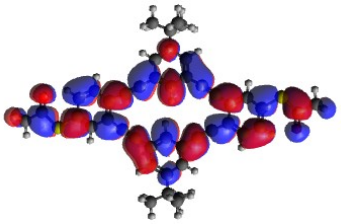

$HOMO - 2 = -5.16\ eV$

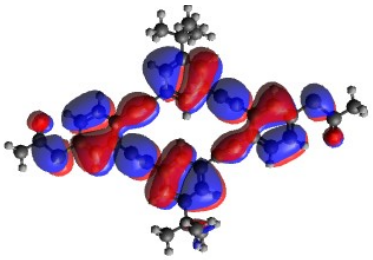

$LUMO + 2 = -1.81\ eV$

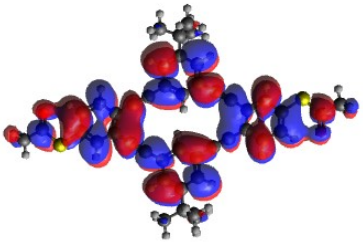

Figure S 3: Top panel: *BMC1* geometry fully optimised. **Lower panel:** cross-linked 1's HOMO, LUMO, HOMO-1, LUMO+1, HOMO-2, and LUMO+2 along with their respective energies.

BMC2

$E_F = -3.83\ eV$

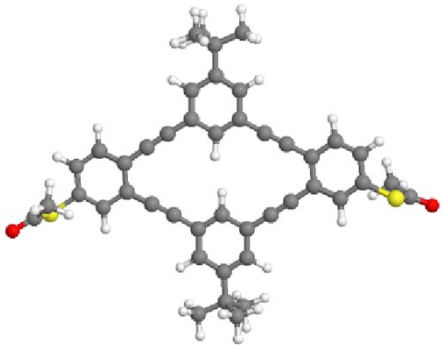

$HOMO = -4.93\ eV$

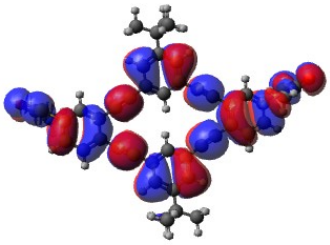

$LUMO = -2.68\ eV$

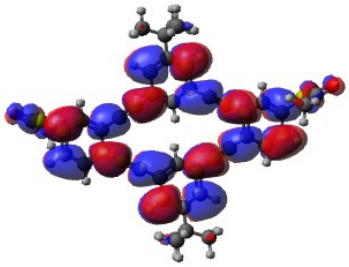

$HOMO - 1 = -5.09\ eV$

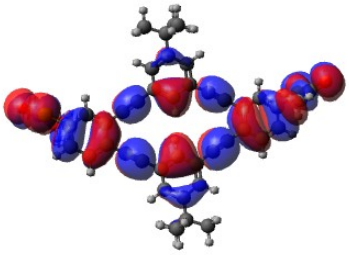

$LUMO + 1 = -2.44\ eV$

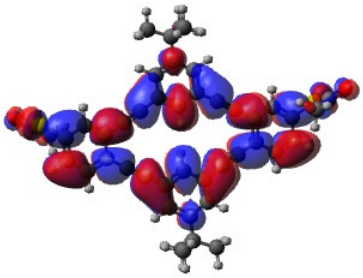

$HOMO - 2 = -2.68\ eV$

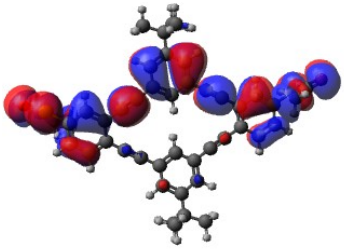

$LUMO + 2 = -2.12\ eV$

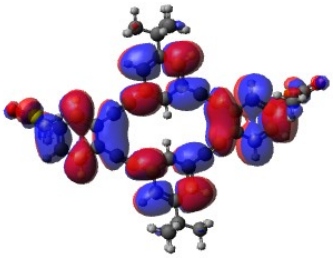

Figure S 4: Top panel: *BMC2* geometry fully optimised. **Lower panel:** cross-linked 1's HOMO, LUMO, HOMO-1, LUMO+1, HOMO-2, and LUMO+2 along with their respective energies.

TMC3

$E_F = -3.36\ eV$

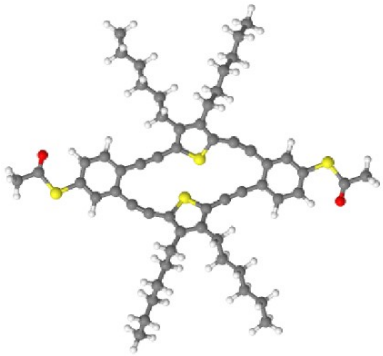

$HOMO = -4.14\ eV$

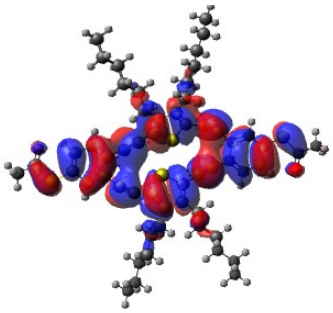

$LUMO = -2.54\ eV$

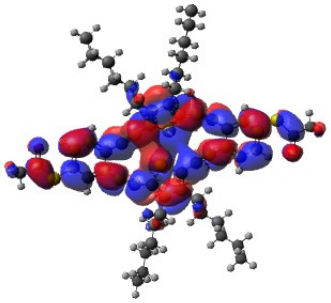

$HOMO - 1 = -4.66\ eV$

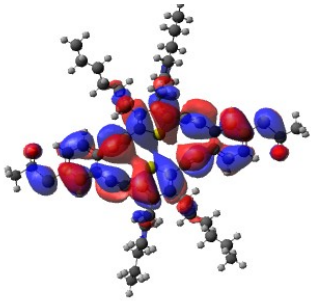

$LUMO + 1 = -1.98\ eV$

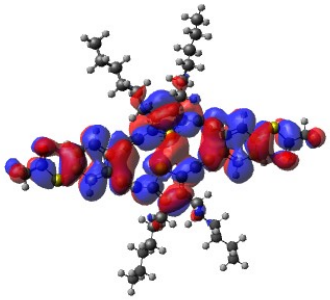

$HOMO - 2 = -5.16\ eV$

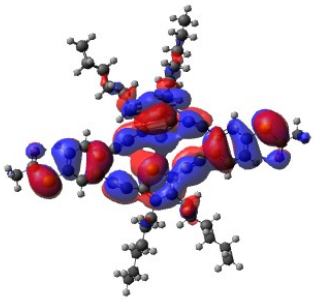

$LUMO + 2 = -1.74\ eV$

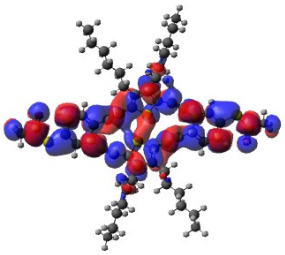

Figure S 5: Top panel: *TMC3* geometry fully optimised**. Lower panel:** cross-linked 1's HOMO, LUMO, HOMO-1, LUMO+1, HOMO-2, and LUMO+2 along with their respective energies.

TMC4

$E_F = -3.68\ eV$

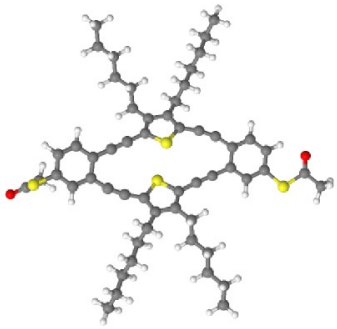

$LUMO = -2.77\ eV$

$HOMO = -4.31\ eV$

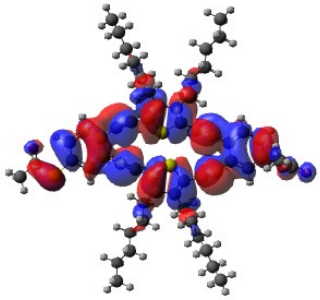

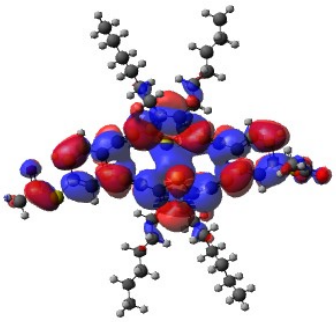

$LUMO+1 = -2.01\ eV$

$HOMO-1 = -4.84\ eV$

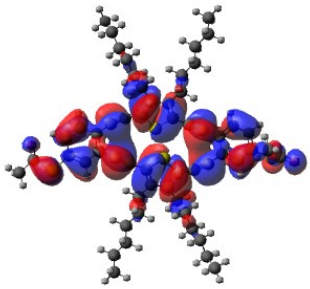

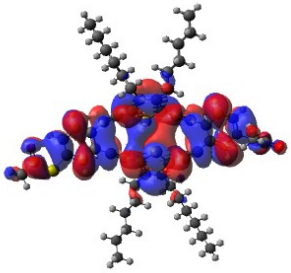

$LUMO+2 = -1.89\ eV$

$HOMO-2 = -5.11\ eV$

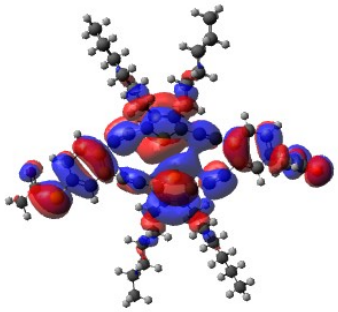

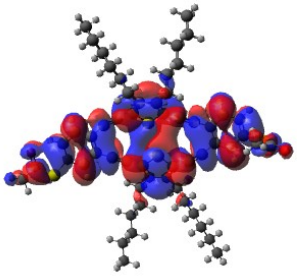

Figure S 6: Top panel: *TMC4* geometry fully optimised. **Lower panel:** cross-linked 1's HOMO, LUMO, HOMO-1, LUMO+1, HOMO-2, and LUMO+2 along with their respective energies.

1.4 Product rule application

To determine whether an orbital product rule can be used to predict whether the quantum interference is constructive or destructive, we apply the product rule based on the observed wavefunction phases at the anchoring positions. The product rule is applied using the signs at the anchoring positions for each orbital as shown in Table S2. A "+" means the signs are the same, and a "–" means the signs are different [4] [5,6].

Rule:

- Same sign (+) → product is positive → Destructive Quantum Interference (D)
- Different sign (–) → product is negative → Constructive Quantum Interference (C)

Table S 2: Product rule table of Macrocycles [1,2,3] and [4] showing the sign comparison and resulting interference.

Structure of Macrocycle with labelled anchor positions (1 and 2).	HOMO	LUMO	OPR prediction
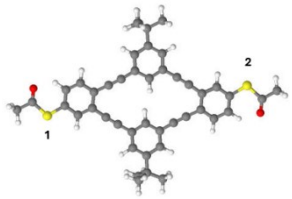	−	+	**C**
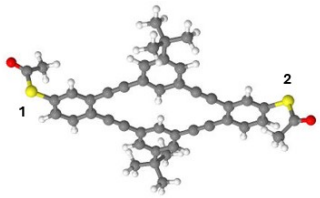	−	−	**D**
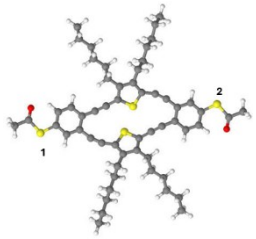	−	−	**D**
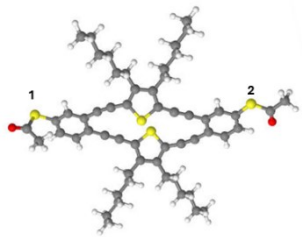	−	+	**C**

1.5 Binding energy

This section presents the binding energy calculations for the four studied macrocycles, focusing on their interaction with Au leads through thiol anchoring groups. All molecules form bonds between the terminal thiol groups and gold electrodes (Au). The density functional theory (DFT) method was employed in conjunction with the counterpoise correction to eliminate the basis set superposition error (BSSE). The binding energy ($B.E$) is computed as the difference between the total energy of the combined system (E_{AB}) and the sum of the energies of the individual components (E_A and E_B), each computed in the presence of ghost atoms [7,8 9]:

$$Binding\ Energy = E_{AB} - E_A - E_B$$

1.5.1 Binding energy of Au-S

Among the four macrocycles, *BMC1* and *2* exhibit identical binding behaviour due to their matching side groups and symmetric structure. Similarly, *TMC3* and *4* share the same edge topology and display equal binding results. The calculated optimised distances and corresponding binding energies are presented in **Figure S 7** and **Figure S 8**, and the summarized numerical values are shown in Table S3 below.

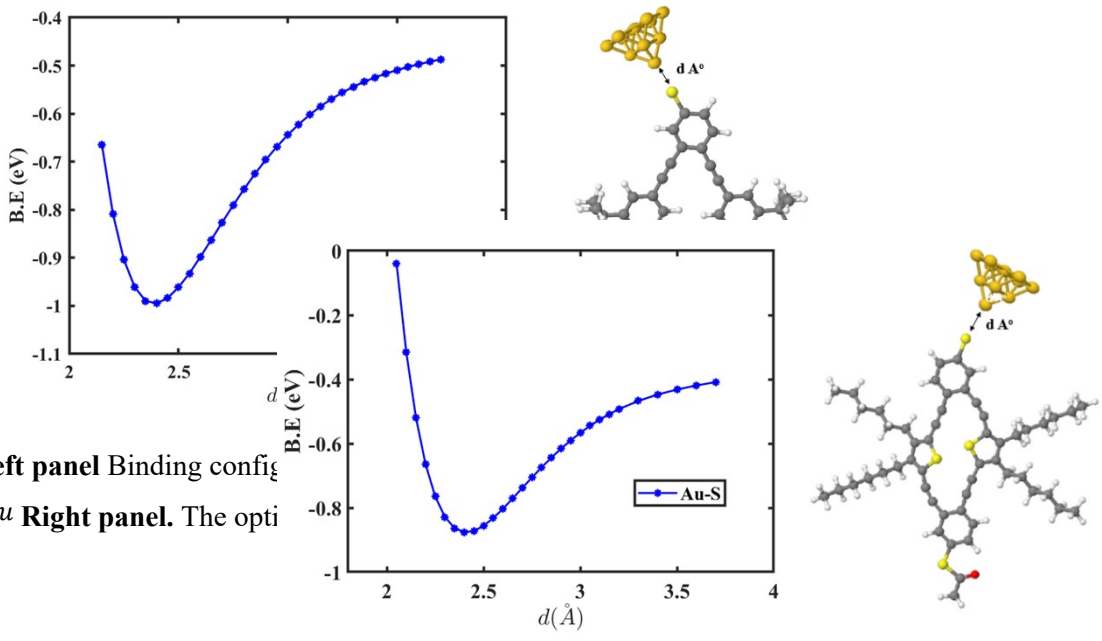

Figure S 7: Left panel Binding config
anchoring to Au **Right panel.** The opti

Figure S8: Left panel Binding configurations and energy curve for *TMC3* and *TMC4*, showing thiol anchoring to *Au* **Right panel**. The optimized distance is 2.4 Å with a binding energy of $-0.88\ eV$.

Table S 3: Summary of optimised binding distances and binding energies for macrocycles $1-4$.

Molecule(s)	Optimised Distance (Å)	Binding Energy (eV)
BMC1 and *2*	2.4	− 0.99
TMC3 and *4*	2.4	− 0.88

1.7 Transmission coefficient $T(E)$

This section investigates the transmission function of four macrocyclic molecules with symmetric and asymmetric designs. The transmission coefficient curves $T(E)$ were obtained using the Gollum quantum transport code, based on the output wavefunction data from DFT calculations.

All structures were connected to gold (Au) electrodes through thiol anchoring groups. To ensure proper anchoring geometry, the acetyl protection group ($-COCH_3$) was removed from the terminal thiol groups [10]. This deprotection step is chemically justified, as the acetyl group detaches spontaneously upon contact with the gold surface during experimental transport measurements, forming direct $Au–S$ bonds.

To interpret the transmission characteristics, we classify molecules as HOMO- or LUMO-dominated based on the alignment of the Fermi level relative to molecular orbitals. A HOMO-dominated system has its transmission peak near the HOMO resonance, favouring hole transport, while a LUMO-dominated system would feature transmission near the LUMO level, supporting electron transport.

our macrocycles exhibit HOMO-dominated electronic characteristics based on their transmission spectra as shown in **Figure S 9**. Among them, *BMC1* and *TMC3* display symmetric macrocyclic frameworks, while *BMC2* and *TMC4* show asymmetric configurations.

The shared HOMO-dominated nature across all four systems suggests that electronic transport is primarily governed by the highest occupied molecular orbital, although the differences in molecular symmetry may contribute to variations in conductance behaviour and interference patterns.

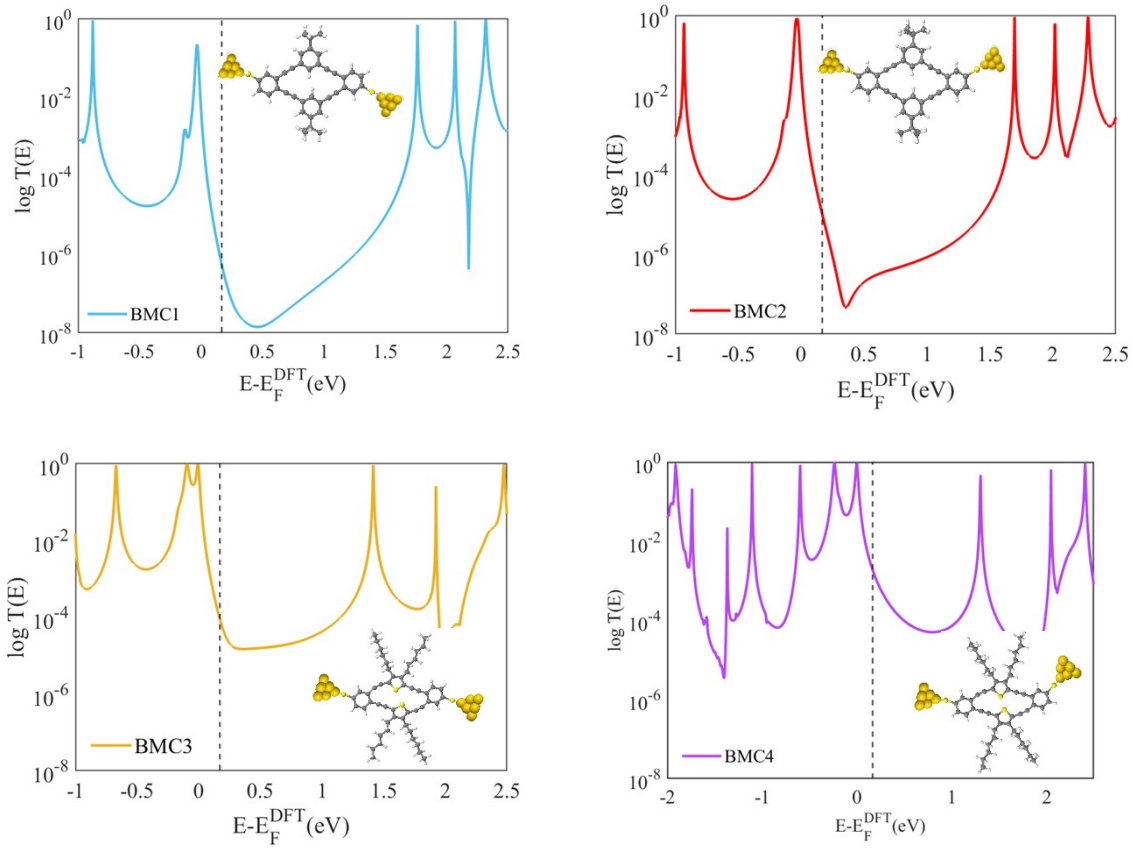

Figure S 9: Schematic illustration and transmission coefficient $T(E)$ of *BMC1-BMC4*. The transmission coefficient $T(E)$ of $Au/S/Au$ junctions against electron energy E is shown in each panel alongside the molecular structure.

results

In this section, we compare the predictions obtained from the product rule with the actual transmission coefficient results derived from DFT-based transport calculations. The product rule provides qualitative predictions about the presence of constructive or destructive quantum interference based on wavefunction signs at the anchoring positions. Transmission spectra offer quantitative insight by revealing dips that indicate destructive interference (DQI) or smooth curves indicating constructive interference (CQI). While the product rule is a powerful

predictor, only around 50% agreement was observed with the DFT results. This partial match is primarily due to orbital degeneracy and complex electronic interactions that are not captured in phase-based analysis alone. As shown in **Figure S 9**, the transmission curves visually support this interpretation. results compare the transmission coefficients $T(E)$ as a function of electron energy E for the four molecules. The Fermi level E_F is set at $0.17\ eV$ in all simulations. The curves illustrate the differences in quantum interference behaviour, with noticeable dips indicating destructive interference (DQI) and smooth transitions indicating constructive interference (CQI). These results are used to compare with the product rule predictions in Table S4.

Table S4: Comparison between product rule predictions and transmission coefficient (**Figure S 9**) outcomes for molecules 1–4 (Note: ✓: OPR and DFT agree while x: OPR and DFT don't agree).

Molecule	OPR	$T(E)$ Observation	OPR and DFT agreement
BMC 1	C	Clear dip observed	x
BMC 2	D	Clear dip observed	✓
TMC 3	D	Smooth curve	x
TMC 4	C	Smooth curve	✓

As shown in the summary table S4, *BMC2* and *TMC4* display agreement between the product rule and transmission coefficient results, whereas, *BMC1* and TMC*3* shows disagreement between them, reflecting the fact that such a rule is merely an approximation (4).

➢ Comparison between experimental and theoretical conductance

The comparison between the experimental and theoretical conductance values for the four macrocycles is summarised in the table below. Theoretical conductance was determined based on the $Au-S$ bonding configuration extracted from the relaxed geometries of each molecule. Experimental conductance was obtained from measured values at room temperature [10]. **Table S5** shows the comparison between the average experimental conductance and theoretical conductance for the four macrocycles. The Fermi level was set at 0.17 eV to ensure consistency with the experimental conductance peak positions.

Table S5: Shows experimental conductance vs average and theoretical conductance for molecules 1–4

Molecule	Junction	Average Experimental Conductance	DFT Junction
BMC1	$S-Au$	− 6.42	− 6.27
BMC2		− 5.82	− 5.02
TMC3		− 4.55	− 4.03
TMC4		− 4.70	− 2.74

1.8 Seebeck coefficient

The Seebeck coefficient S, (also known as thermopower), measures the voltage generated across a molecular junction in response to a temperature difference between the electrodes. In molecular electronics, S provides valuable information about the type of dominant charge carriers (holes or electrons) and the alignment of frontier orbitals relative to the Fermi energy EF. Within the Landauer formalism, and under the assumption that the transmission function $T(E)$ varies smoothly near E_F, the Seebeck coefficient can be approximated by the Mott formula [11]:

$$S = -\frac{\pi^2 k_B^2 T}{3e} \frac{\partial \ln(T(E))}{\partial E}\bigg|_{E=E_F}$$

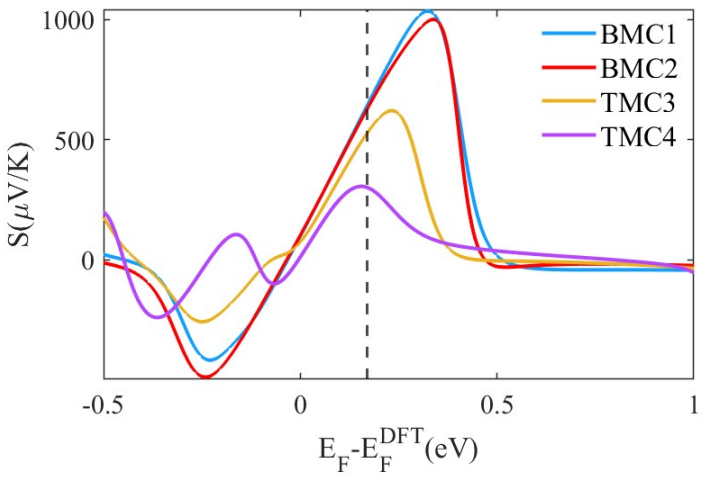

Figure S10: Seebeck coefficient S as a function of the Fermi energy for the molecular junctions $BMC1$, $BMC2$, $TMC3$, and $TMC4$, with corresponding values at the Fermi level of $643, 628, 527, and\ 300\ \mu V/K$, respectively.

Here, k_B is Boltzmann's constant, T is temperature, and e is the elementary charge. The sign and magnitude of S depend on the slope of the transmission function near the Fermi level. A positive S implies that hole transport dominates (HOMO-dominated), while a negative S suggests electron transport (LUMO-dominated). The Seebeck profiles shown in **Figure 10** reflect this behaviour, with noticeable variations across the four macrocycles due to their differing symmetry and orbital alignment. These findings offer additional confirmation of the HOMO/LUMO nature already observed in the transmission spectra.

All four molecules exhibit a predominantly positive Seebeck coefficient around the Fermi level, indicating that hole transport dominates. This behaviour aligns with the HOMO-dominated nature of the transmission spectra observed for each molecule, where the Fermi energy lies closer to the highest occupied molecular orbital.

We compared the Seebeck coefficients obtained for our macrocyclic molecules with values reported for linear, single-branch analogues in a recent study by ref [12]. (see **Table S6** for comparison). Their 2,5-TP-SAc and para-OPE3 compounds, which share similar thiophene and benzene backbones with our systems but involve only a single conduction pathway, exhibited Seebeck coefficients below 10 μV/K. In contrast, our macrocyclic, multi-branch structures BMC1 to TMC4 exhibited significantly higher Seebeck values, ranging from +300 μV/K up to +643 μV/K. This represents an enhancement of nearly 100 times higher compared to the single-branch counterparts. These findings underscore the beneficial role of cyclic topology and quantum interference in enhancing thermoelectric performance.

Table S6: Seebeck coefficients (S) for single-branch molecules (Wenjing Hong *et al.*) vs. our cyclic, multi-branch systems.

Single-Branch (ref [12] study)	**S (μV/K)**	**Our Study (Cyclic, Multi-Branch)**	**S (μV/K)**
2,4-TP-SAc	$+12.36 \pm 0.65$	$BMC1$	$+643$
2,5-TP-SAc	$+7.97 \pm 0.26$	$BMC2$	$+628$
2,5-TP-Py	-7.56 ± 0.69	$TMC3$	$+527$
para-OPE3	$+7.78 \pm 0.34$	$TMC4$	$+300$

1.9 Sulfur repositions in thiophene rings (TMC3 and TMC4)

To further examine the role of thiophene substitution on quantum interference, we explored a set of hypothetical modifications to TMC3 and TMC4, involving repositioning the sulfur atoms within the thiophene rings, while preserving the anchoring groups. Based on discussions with our synthetic collaborators, these structural rearrangements are considered chemically feasible and may be experimentally realizable. Following the same approach as in our conventional DFT calculations, each modified molecule was fully relaxed via geometry optimization, and DFT-based binding energy analysis was carried out to assess structural stability. Additionally, we performed Frontier Orbital Analysis to examine the electronic distribution and its influence on quantum transport properties.

We calculated the Seebeck coefficient for the sulfur-repositioned structures, and the results show relatively higher Seebeck values compared to the original molecules. The Seebeck calculation curves are shown in **Figure S11**, and **Table S7** represents the corresponding Seebeck coefficient values.

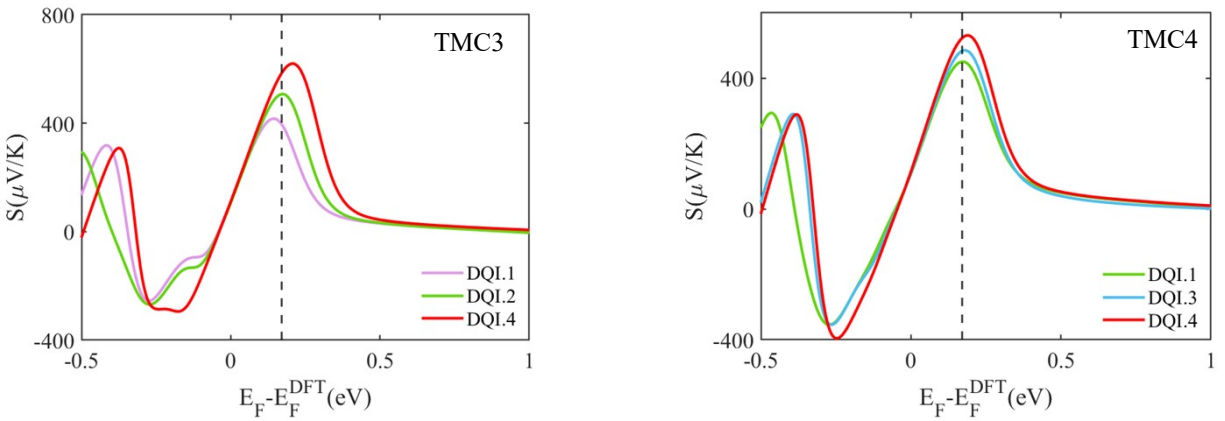

Figure S11: Seebeck coefficient S as a function of the Fermi energy for TMC3 and TMC4, including their adjusted variants (DQI.1 – DQI.4)

Table S7. Calculated Seebeck (S) values at $E - E_F^{DFT} = 0.17$ eV for the sulfur-repositioned macrocycles TMC3 and TMC4. The DQI-adjusted variants exhibit higher S values,

Molecule	Structural Varient	S (μV/K)
$TMC3$	DQI.1	+ 396.9
	DQI.2	+ 507
	DQI.4	+ 583.6
$TMC4$	DQI.1	450.5
	DQI.3	+ 483.2
	DQI.4	+ 522.4

2. References

(1) Soler, J. M.; Artacho, E.; Gale, J. D.; García, A.; Junquera, J.; Ordejón, P.; Sánchez-Portal, D. The SIESTA Method for Ab Initio Order-N Materials Simulation. *J. Phys. Condens. Matter* **2002**, *14* (11), 2745. https://doi.org/10.1088/0953-8984/14/11/302.

(2) Artacho, E.; Anglada, E.; Diéguez, O.; Gale, J. D.; García, A.; Junquera, J.; Martin, R. M.; Ordejón, P.; Pruneda, J. M.; Sánchez-Portal, D.; Soler, J. M. The SIESTA Method; Developments and Applicability. *J. Phys. Condens. Matter* **2008**, *20* (6), 064208. https://doi.org/10.1088/0953-8984/20/6/064208.

(3) Sánchez-Portal, D.; Ordejón, P.; Artacho, E.; Soler, J. M. Density-Functional Method for Very Large Systems with LCAO Basis Sets. *Int. J. Quantum Chem.* **1997**, *65* (5), 453–461. https://doi.org/10.1002/(SICI)1097-461X(1997)65:5%253C453::AID-QUA9%253E3.0.CO;2-V.

(4) Lambert, C. J.; Liu, S.-X. A Magic Ratio Rule for Beginners: A Chemist's Guide to Quantum Interference in Molecules. *Chem. – Eur. J.* **2018**, *24* (17), 4193–4201. https://doi.org/10.1002/chem.201704488.

(5) Lambert, C. J.; Raimondi, R. Phase-Coherent Transport in Hybrid Superconducting Nanostructures. *J. Phys. Condens. Matter* **1998**, *10* (5), 901. https://doi.org/10.1088/0953-8984/10/5/003.

(6) Geng, Y.; Sangtarash, S.; Huang, C.; Sadeghi, H.; Fu, Y.; Hong, W.; Wandlowski, T.; Decurtins, S.; Lambert, C. J.; Liu, S.-X. Magic Ratios for Connectivity-Driven Electrical Conductance of Graphene-like Molecules. *J. Am. Chem. Soc.* **2015**, *137* (13), 4469–4476. https://doi.org/10.1021/jacs.5b00335.

(7) Kobko, N.; Dannenberg, J. J. Effect of Basis Set Superposition Error (BSSE) upon Ab Initio Calculations of Organic Transition States. *J. Phys. Chem. A* **2001**, *105* (10), 1944–1950. https://doi.org/10.1021/jp001970b.

(8) *Counterpoise Correction and Basis Set Superposition Error | PDF | Intermolecular Force | Molecules*. Scribd. https://www.scribd.com/document/421508846/cp (accessed 2025-06-01).

(9) Boys, S. F.; and Bernardi, F. The Calculation of Small Molecular Interactions by the Differences of Separate Total Energies. Some Procedures with Reduced Errors. *Mol. Phys.* **1970**, *19* (4), 553–566. https://doi.org/10.1080/00268977000101561.
(10) Design and Synthesis of Multipath Compact Cyclophanes for Quantum Interference Studies. *Eur. J. Org. Chem.* **2024**, e202400914. https://doi.org/10.1002/ejoc.202400914.
(11) J. Lambert, C. Basic Concepts of Quantum Interference and Electron Transport in Single-Molecule Electronics. *Chem. Soc. Rev.* **2015**, *44* (4), 875–888. https://doi.org/10.1039/C4CS00203B.
(12) Chen, H.; Chen, Y.; Zhang, H.; Cao, W.; Fang, C.; Zhou, Y.; Xiao, Z.; Shi, J.; Chen, W.; Liu, J.; Hong, W. Quantum Interference Enhanced Thermopower in Single-Molecule Thiophene Junctions. *Chin. Chem. Lett.* **2022**, *33* (1), 523–526. https://doi.org/10.1016/j.cclet.2021.06.052.